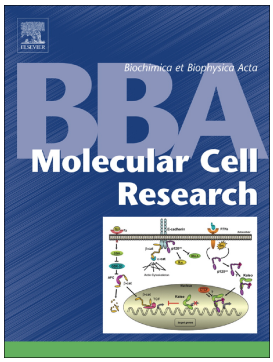

Mining of Ebola virus entry inhibitors identifies approved drugs as two-pore channel pore blockers

Christopher J. Penny, Kristin Vassileva, Archana Jha, Yu Yuan, Xavier Chee, Elizabeth Yates, Michela Mazzon, Bethan S. Kilpatrick, Shmuel Muallem, Mark Marsh, Taufiq Rahman, Sandip Patel

PII: S0167-4889(18)30499-3
DOI: https://doi.org/10.1016/j.bbamcr.2018.10.022
Reference: BBAMCR 18389

To appear in: *BBA - Molecular Cell Research*

Received date: 4 September 2018
Revised date: 29 October 2018
Accepted date: 31 October 2018

Please cite this article as: Christopher J. Penny, Kristin Vassileva, Archana Jha, Yu Yuan, Xavier Chee, Elizabeth Yates, Michela Mazzon, Bethan S. Kilpatrick, Shmuel Muallem, Mark Marsh, Taufiq Rahman, Sandip Patel , Mining of Ebola virus entry inhibitors identifies approved drugs as two-pore channel pore blockers. Bbamcr (2018), https://doi.org/10.1016/j.bbamcr.2018.10.022

Mining of Ebola virus entry inhibitors identifies approved drugs as two-pore channel pore blockers

Christopher J. Penny[1], Kristin Vassileva[1,2], Archana Jha[3], Yu Yuan[1], Xavier Chee[4], Elizabeth Yates[1], Michela Mazzon[2], Bethan S. Kilpatrick[1], Shmuel Muallem[3], Mark Marsh[2], Taufiq Rahman[4,5] and Sandip Patel[1,6]

[1]Department of Cell and Developmental Biology, University College London, London, UK

[2]MRC Laboratory for Molecular Cell Biology, University College London, London, UK

[3]Epithelial Signaling and Transport Section, National Institute of Dental Craniofacial Research, National Institutes of Health, Bethesda, MD 20892, USA

[4]Department of Pharmacology, University of Cambridge, Cambridge, UK

Correspondence to [5]mtur2@cam.ac.uk or [6]patel.s@ucl.ac.uk

Key words: TPC2; NAADP; Ca^{2+}; lysosomes; virtual screening; Ebola virus

Two-pore channels (TPCs) are Ca^{2+}-permeable ion channels localised to the endo-lysosomal system where they regulate trafficking of various cargoes including viruses. As a result, TPCs are emerging as important drug targets. However their pharmacology is ill-defined. There are no approved drugs to target them. And their mechanism of ligand activation is largely unknown. Here, we identify a number of FDA-approved drugs as TPC pore blockers. Using a model of the pore of human TPC2 based on recent structures of mammalian TPCs, we virtually screened a database of ~1500 approved drugs. Because TPCs have recently emerged as novel host factors for Ebola virus entry, we reasoned that Ebola virus entry inhibitors may exert their effects through inhibition of TPCs. Cross-referencing hits from the TPC virtual screen with two recent high throughput anti-Ebola screens yielded approved drugs targeting dopamine and estrogen receptors as common hits. These compounds inhibited endogenous NAADP-evoked Ca^{2+} release from sea urchin egg homogenates, NAADP-mediated channel activity of TPC2 re-routed to the plasma membrane, and $PI(3,5)P_2$-mediated channel activity of TPC2 expressed in enlarged lysosomes. Mechanistically, single channel analyses showed that the drugs reduced mean open time consistent with a direct action on the pore. Functionally, drug potency in blocking TPC2 activity correlated with inhibition of Ebola virus-like particle entry. Our results expand TPC pharmacology through the identification of approved drugs as novel blockers, support a role for TPCs in Ebola virus entry, and provide insight into the mechanisms underlying channel regulation.

1. Introduction

NAADP is a potent Ca^{2+} mobilizing messenger that triggers Ca^{2+} release from acidic Ca^{2+} stores such as lysosomes [1-5]. Critical to NAADP action are the endo-lysosomal two-pore channels (TPCs) [6-9]. Local Ca^{2+} fluxes through TPCs are increasingly implicated in membrane trafficking events [10, 11]. These include roles for TPCs in regulating lysosome morphology [12], retrograde transport between late endosomes and the Golgi [13], and endocytic trafficking of receptors for LDL and growth factors [14, 15], pigment granules [16] and integrins [17]. They also likely regulate non-vesicular trafficking by strengthening membrane contacts sites between late-endosomes and the ER [18]. Consequently, TPCs are fast emerging as potential therapeutic targets in diverse disorders such as Parkinson's disease, fatty liver disease and cancer [12, 14, 17, 19]. Moreover, TPCs have been identified as novel host factors for Ebola virus (EBOV) entry [20]. This virus enters cells through macro-pinocytosis, traffics through the endo-lysosomal system and, following binding to its intracellular receptor NPC1 [21], fuses with late endosomes/lysosomes to release its genome into the cytoplasm. Molecular or chemical inhibition of TPCs prevents EBOV infection likely at a late entry step, although the mechanism is unclear [20, 22].

TPCs are dimeric ion channels, comprising a duplicated domain architecture, which are likely a bridge during the evolution four-domain voltage-gated Ca^{2+} and Na^{+} channels [23-25]. Atomic structures of plant [26-28] and mammalian [29, 30] channels are emerging providing detailed insight into the architecture of the pore. Two isoforms (TPC1 and TPC2) found in humans localise to distinct compartments within the endo-lysosomal system [9, 31]. TPC2 is predominantly localised to late endosomes and lysosomes through an N-terminal targeting motif, which when mutated results in rerouting of the channel to the plasma membrane [32]. The activation mechanisms and ion selectivities of TPCs are areas of active investigation [33, 34]. Although many studies have shown TPCs are required for NAADP-mediated Ca^{2+} signalling, NAADP appears to interact with TPCs indirectly through putative binding proteins [35-38]. In contrast, the endo-lysosomal lipid $PI(3,5)P_2$ has emerged as a direct channel activator that binds within the first domain of TPCs [29, 30, 39]. Interestingly, residues in the S4-S5 linker within this domain required for NAADP-mediated Ca^{2+} signals [40] fall within the $PI(3,5)P_2$ binding site [29] indicating a complex interplay between small molecule activators and accessory proteins.

Despite the growing pathophysiological importance of TPCs, there are currently few selective chemical tools to inhibit NAADP/TPC signalling. BZ194 [41], a N-alkylated nicotinic acid derivative, and Ned-19 [42], identified through a ligand-based virtual screen, are cell-permeable inhibitors of NAADP-evoked Ca^{2+} signals. But their indirect action, coupled with potentially promiscuous actions of their target NAADP-binding proteins on other channels [43], complicates the use of NAADP antagonists in a physiological setting. This underscores the need for direct channel inhibitors. We recently used a combination of homology modelling, molecular docking analyses and Ca^{2+} measurements to show that TPCs are likely to be direct targets for a number of voltage-gated Ca^{2+} and Na^{+} channel modifiers [24]. Tetrandrine [20], another Ca^{2+} channel antagonist has also recently emerged as a TPC blocker and potent inhibitor of EBOV entry. Finally, the flavonoid naringenin [44] has been shown to block TPCs, but with low affinity. Both tetrandrine and naringenin have multiple targets and are not approved for human use world-wide. There are therefore a limited number of drugs that directly inhibit TPCs.

Here, we apply a combination of structural modelling, virtual screening, Ca^{2+} measurements, electrophysiology and virus entry assays to identify approved drugs that both inhibit EBOV entry and block TPC activity.

2. Methods

2.1 Virtual screening

The structure of human TPC2 (Uniprot accession: Q8NHX9) in an open conformation was modelled on the cryoEM structure of $PI(3,5)P_2$-bound mouse TPC1 (pdb: 6C9A) [29] using SWISS-MODEL [45]. The first 40 residues were excluded due to lack of appropriate template. The final model was chosen using the default local model quality estimation method (QMEANDisCo) based on a novel version of QMEAN [45]. Additional model refinement was performed using GalaxyRefine [46].

A conformer library for the e-Drugs3D-2017 drug set [47] was prepared using Omega v3.0.1.2 (OpenEye Scientific Software, Santa Fe, NM). MakeReceptor (OEDOCKING 3.2.0.2; OpenEye Scientific Software, Santa Fe, NM) was used to generate the active site for virtual screening. This was centred on the pore vestibule and extended from above the selectivity filter to below the bundle crossing (40 x 40 x 77 µm). The starting pose was based on blind docking of verapamil using AutoDock Vina [48] with an exhaustiveness value of 24. Screening was carried out with FRED (OEDOCKING 3.2.0.2; OpenEye Scientific Software, Santa Fe, NM) using default parameters returning the top 10000 conformers ranked by the Chemgauss4 score (Table S1). All but the top ranked conformer for each ligand were excluded. This analysis retrieved 1480 unique drugs and their metabolites. The top 200 are listed in Table S1.

Enrichment analysis of the top hits was performed by dividing the proportion of a given drug class within the top 200 hits by the proportion of that class in the screen as a whole. Drugs were classified according to their annotated primary target in eDrugs3D. This analysis was limited to classes where there were more than 3 drugs. A class was considered enriched if values were > 1.5.

2.2 Ca^{2+} measurements

Ca^{2+} release assays using sea urchin egg homogenates were performed as described previously [49]. Briefly, egg homogenates were loaded with Ca^{2+} by sequential dilution in a cytosol-like medium supplemented with an ATP-regenerating system. Medium Ca^{2+} concentration was monitored fluorimetrically with Fluo-4.

2.3 Single channel current recording

Patch clamp recording in the excised inside-out configuration was performed as described in [32] using HEK cells expressing human TPC2 tagged with GFP at its C-terminus and where leucines 11 and 12 were replaced with alanine to promote cell surface targeting. The pipette (luminal) solution contained (in mM): 145 NaCl, 5 KCl, 2 $CaCl_2$, 1 $MgCl_2$, 10 HEPES and 10 MES (pH adjusted to 4.6 with NaOH). The bath (cytoplasmic) solution had the same composition except MES was excluded and pH was adjusted to 7.2 with NaOH. Osmolarity of the solutions was adjusted to ~300 mOsm with glucose.

The methods used for recording and analyzing currents were reported previously [50]. Pipettes were coated with Sigmacote™, fire polished and minimally filled with the pipette solution. Currents were amplified using an Axopatch 200B amplifier, filtered at 1 kHz (-3 dB) with an internal 4-pole Bessel filter and digitized at 10 kHz with a Digidata 1322A interface

and pClamp 10 suite. Unless otherwise stated, all recordings were at a holding potential of +40 mV.

For determining unitary current amplitude and unitary conductance, currents were analyzed using the 50% threshold crossing criterion using ClampFit 10 and openings briefer than 700 μs (twice the filter rise time) were excluded from the analysis [51]. Due to uncertainty about the number of channels in most recordings, channel activity was expressed as NP_o.

For kinetic analyses of single channel records, a simple two state scheme (C ⇆ O) was initially used to idealize currents at full bandwidth (1 kHz) using the segmental k-means (SKM) hidden-Markov algorithm implemented in QuB [52]. Additional states were then systematically added to the initial scheme with various topologies using the MIL module of QuB. A dead time of 200 μs was retrospectively imposed to correct for missed events [51]. MIL fits a gating scheme to the single channel records and optimises the rate constants based on a maximum likelihood-based Markovian approach. The final gating schemes were derived when further changes in either the number of states or their connectivity did not produce significant (≥10) increment in the log likelihood (LL) ratio [50, 52]. Closed time distributions were analysed when channel activity was reasonably high (NP_o>0.15) and when only openings to a single current level were evident over a duration of ≥5 min [53].

Analyses were performed 10-15 s following NAADP/drug application in the bath solution to ensure adequate mixing.

2.4 Whole lysosomal current recording

Lysosomal currents were recorded using a modified patch clamp procedure as described in [54] and COS-7 cells expressing human TPC2 tagged with GFP at its C-terminus [7]. Briefly, cells were treated with 1 μM vacuolin-1, for 1–2 h and the resulting enlarged lysosomes accessed by breaking the plasma membrane with a glass pipette. The pipette (luminal) solution and bath (cytoplasmic) solution contained (in mM): 140 NaCl, 5 KCl, 10 HEPES (pH 7.4 with NaOH). After formation of a GΩ seal with a lysosome, break in was achieved by quick voltage steps of +350 mV. Current was measured with an Axopatch 200B patch clamp amplifier that was controlled by pCLAMP9 software. The current protocol used 400-ms rapid alterations of membrane potential (RAMP) from −100 to +100 mV from a holding potential of 0 mV at 4 s intervals. The currents were filtered at 1 kHz with an internal four-pole Bessel filter, sampled at 5 kHz, and stored to a hard drive by Digidata 1440.

2.5 Ebola virus-like-particle entry assays

Virus-like particles (VLPs) for EBOV were generated as described in [55]. Briefly, HEK293T cells were co-transfected with constructs encoding the EBOV matrix protein, VP40, tagged with a β-lactamase reporter at its N-terminus [56] and the EBOV glycoprotein (GP; strain Zaire) [57], both a kind gift from Adolfo Garcia-Sastre. Cells were maintained in DMEM supplemented with 10% (v/v) FBS, 100 μg/mL streptomycin and 100 units/mL penicillin at 37^{o}C in a humidified atmosphere containing 5% CO_2. Culture media were harvested after 48h, cleared by centrifugation and VLP-containing supernatants stored at -80^{0}C until use.

The VLP entry assay [55] was adapted and optimised to a 96-well plate format. HeLa Kyoto cells were seeded at a density of 8x10^3 cells/well and maintained for 40 h prior to drug treatment in DMEM supplemented with 10% (v/v) FBS, 100 μg/mL streptomycin and 100 units/mL penicillin at 37^{0}C in a humidified atmosphere containing 5% CO_2. Cells were incubated with drugs in DMEM + 2% (v/v) FBS for 1 h under culture conditions prior to the addition of VLPs (1:2 dilution). Cells were spinoculated at 450 x *g* for 1 h at 4^{o}C, followed by

incubation for 3 h under culture conditions to allow VLP entry in the continued presence of drugs. Cells were washed once with CO_2-independent medium supplemented with 10% (v/v) FBS and 1% (v/v) L-glutamine and loaded with the β-lactamase substrate, CCF2 (LiveBLAzer FRET–B/G Loading Kit, Invitrogen) according to the manufacturer's instructions using the alternative substrate loading protocol. Cells were trypsinised, fixed with 1% paraformaldehyde for 20 min and analysed by flow cytometry using a LSRII flow cytometer (Becton Dickinson, USA) collecting at least 10,000 events. β-lactamase activity was assessed in live cells with the FlowJo software package by determining the proportion of blue fluorescent cells (cleaved substrate; excitation 405 nm) relative to green fluorescent cells (total substrate; excitation 488 nm) using filter sets for Pacific-blue and FITC, respectively.

2.7 Data analysis

Data are presented as mean values +/- standard error of the mean where indicated. Concentrations that caused 50% inhibition (IC_{50}) and Hill coefficients (n_H) were derived from fitting of inhibition curves using KaleidaGraph (Synergy sotware).

Results

3.1 Identification of putative TPC2 inhibitors through a structure-based virtual screen of approved drugs based on the TPC2 pore

Recent advances in the structural biology of TPCs [28, 30] provide novel opportunities to gain insight into TPC pharmacology. We thus applied a structure-based virtual screening approach to identify novel lead compounds targeting the TPC pore. We took advantage of the recent cryo-EM structure of a mammalian TPC [29] to model the pore of human TPC2. (Fig. 1A) and used this model to perform an *in silico* screen of the e-Drugs3D database, which consists of ~ 1500 drugs approved by the FDA for use in humans. The results of this screen are depicted schematically in Fig. 1B where each compound is ranked according to its Chemguass4 score. This score is a measure of the predicted strength of interaction whereby more negative values indicate a stronger predicted interaction.

Our previous targeted docking analyses showed that voltage-gated Ca^{2+} and Na^{+} channel blockers likely interact with the TPC pore through a common 'ancestral' binding site [24]. Of the Ca^{2+} channel blockers analysed previously, nicardipine was predicted to interact most strongly with the pore and diltiazem was the most potent functionally [24]. Accordingly, nicardipine and diltiazem were recovered as top ranking blockers in the present screen (Fig. 1C, asterisk). Additionally, the mean rank and mean Chemguass4 scores of all Ca^{2+} channel blockers in the screen were lower than for Na^{+} channel blockers (Fig 1 C-D). This accords with our docking and functional analyses showing more avid interaction and more potent inhibition of TPCs by blockers of Ca^{2+} relative to Na^{+} channels [24]. Taken together, these analyses support our unbiased approach for identification of TPC inhibitors.

Subsequent efforts were focused on the top 200 hits recovered in the virtual screen. We performed enrichment analysis according to the primary target where annotated. As shown in Fig. 1D, this analysis revealed a number of drugs targeting different G-protein coupled receptors, HMG-CoA reductase, the estrogen receptor and the angiotensin II converting enzyme. This unbiased approach thus returns a number of drugs within distinct drug classes that potentially target the TPC2 pore.

3.2 Prioritisation of approved drugs that inhibit Ebola virus entry as putative TPC2 inhibitors

Because TPCs have emerged as novel host factors for EBOV infection [20], we reasoned that some of the FDA-approved drugs recently highlighted in high-throughput screens as EBOV entry inhibitors might function as TPC blockers. We thus compared our top 200 hits with two recent anti-EBOV screens [58, 59] that together identified 73 unique EBOV entry inhibitors (Fig. 2A). Of these, 51 were present in e-Drugs3D and all but 5 were recovered in the TPC virtual screen (Fig. 2B). Notably, approximately, a third of these (14) ranked within the top 200 of the TPC screen (Fig. 2C). Inspection of the prioritised hit compounds (Fig. 2D) revealed the Ca^{2+} channel blocker bepridil, further underscoring this class of compounds as TPC blockers. Importantly, this analysis also returned 4 dopamine receptor antagonists and 5 selective estrogen receptor modulators (SERMs). The prevalence of drugs in these two classes is consistent with our enrichment analysis from the TPC screen (Fig. 1D). Thus, virtual screening against the TPC2 pore and physical screening for EBOV entry inhibitors converge on dopamine receptor antagonists and SERMs as candidate TPC inhibitors.

3.3 Dopamine antagonists and selective estrogen receptor modulators block endogenous NAADP-mediated Ca^{2+} signals

To examine the functionality of the drugs as TPC inhibitors, we first tested their effects on Ca^{2+} signals evoked by NAADP. We used sea urchin egg homogenates for this analysis as this preparation is considered the 'gold standard' for assessing NAADP-mediated Ca^{2+} signalling [60]. As shown in Fig. 3A, NAADP mediated a robust Ca^{2+} signal that was largely blocked by bepridil (100 µM). Similar results were obtained with fluphenazine and pimozide, both dopamine receptor antagonists (Fig. 3A). We also tested the effects of the SERMs, raloxifene and clomiphene on NAADP responsiveness. Raloxifene almost completely blocked NAADP-evoked Ca^{2+} release whereas clomiphene effected a partial block (Fig. 3A).

The inhibitory effects of all these drugs were concentration dependent (Fig. 3B) with the following IC_{50} and n_H values: bepridil (33 µM, 1.5), fluphenazine (42 µM, 1,3), pimozide (42 µM, 0.96), raloxifene (28 µM, 1.6) and clomiphene (94 µM, 1.7). To determine selectivity, we examined the effects of the drugs on Ca^{2+} release by cyclic ADP-ribose, which mediates its effects through the ryanodine receptor. As summarized in Fig. 3C, all drugs were less effective at inhibiting responses to cyclic ADP-ribose than NAADP, attesting to specificity.

Taken together, these data identify dopamine receptor antagonists and SERMs as novel inhibitors of NAADP action consistent with their predicted interaction with TPCs.

3.4 Dopamine antagonists and selective estrogen receptor modulators inhibit single channel activity of TPC2 by reducing open time

To provide more direct evidence that these compounds are TPC blockers and to extend our analyses to mammalian systems, we analysed NAADP-mediated channel activity of human TPC2. We did this using cell surface targeted TPC2 to facilitate single channel recording in a null background. Na^+ was used as the major cation to complement our previous analyses using Ca^{2+} as the permeant ion [32]. As shown in Fig. 4A, some spontaneous activity was noted in most of the excised patches. NAADP addition to the bath solution robustly enhanced channel activity in a concentration dependent manner. Current amplitude histograms are shown in Fig. S1A-C. Summary data quantifying the normalised open probability NP_O is shown in Fig. 4B. Analysis of current-voltage relationships indicated a unitary Na^+ conductance (γ_{Na}) of 86 $\pm$ 0.7 pS (Fig. 4C; n = 3). Single channel openings in the absence and presence of NAADP were best fit by a single exponential with a mean open time of ~ 5 ms (Fig. 4D). For a sub-set of recordings where we were confident that the openings represented a single active channel ($P_o \geq 0.15$, ≥ 5min recording duration) [50], closed time distribution was also analysed (Fig. 4D). The distribution was best fit by a double

exponential with time constants of 0.7 ± 0.4 ms and 47 ± 3.5 ms, constituting 49 ± 1 % and 51 ± 1 % of the distribution, respectively (n = 4). Kinetic modelling yielded two topologies with similar LL ratios that linearly connected the closed states (C_1 and C_2) with the open state (O) (Fig. 4F). Collectively, these data affirm the sensitivity of TPC2 to NAADP and its permeability to Na^+ and provide a framework for assessing drug action at the single channel level.

We used this experimental setting to assess the effects of fluphenazine and raloxifene (representative of the two identified drug classes) on TPC2 channel activity. Fig. 5 shows continuous uninterrupted recordings of TPC2 channel activity in response to NAADP and subsequent addition of the drugs. Both drugs acutely inhibited NAADP-mediated channel activity (Fig. 5A-B). We also tested the effects of the NAADP antagonist Ned-19. As shown in Fig. 5C, Ned-19 also similarly inhibited channel activity. To gain mechanistic insight into drug block, we analysed dwell time distributions. As shown in Fig. 5D-E, both fluphenazine and raloxifene reduced the mean open time from ~ 5 ms to ~ 3 ms without affecting the unitary current sizes. Current amplitude histograms are shown in Fig. S1D-F.These data are consistent with a direct interaction of the drugs with the pore. In contrast, Ned-19 affected neither the mean open time nor unitary current size (Fig. 5F) suggesting a distinct mechanism of action. Data summarizing the effects of the drugs on NP_o, open times and unitary conductance are shown in Fig. 5G. Taken together, these data suggest that fluphenazine and raloxifene effectively behave as pore blockers.

3.5 Dopamine antagonists and selective estrogen receptor modulators inhibit lysosomal TPC2 currents and entry of Ebola virus-like particles with similar potency

Because TPC2 in the plasma membrane may not faithfully reflect the properties of the channel in its native environment, we performed electrophysiological analysis of enlarged lysosomes expressing wildtype TPC2 (Fig. 6). For these experiments, TPC2 was stimulated with a saturating concentration of $PI(3,5)P_2$, which gives larger currents than NAADP in this experimental setting [54] most likely due to a direct interaction with the channel [61]. As shown in Fig. 6A, $PI(3,5)P_2$ stimulated robust currents in TPC2-expressing lysosomes. These responses were inhibited by fluphenazine in a concentration-dependent manner with near full block achieved at 30 µM (Fig. 6A). Raloxifene also inhibited $PI(3,5)P_2$-mediated currents with maximal effects at 3 µM (Fig. 6A). The inhibitory effects of both drugs were reversed upon washout (Fig. 6A) Concentration-effect relationships showed that raloxifene was particularly potent at blocking TPC2 currents IC_{50} = 0.63 µM, n_H = 1.3) in this setting compared to fluphenazine (IC_{50} = 8.2 µM, n_H = 1.3), respectively (Fig. 6B).

Finally, we examined the potency of dopamine receptor antagonists and SERMs on EBOV entry. As a surrogate for EBOV, we used Ebola VLPs carrying β-lactamase. Following fusion mediated by the EBOV glycoprotein, β-lactamase is delivered to the target cell cytoplasm where it mediates cleavage of a fluorescent substrate. Fig. 7A quantifies infection of HeLa cells by the VLPs. Infection was blocked by pre-treatment with EIPA (11.1 µM), an inhibitor of macro-pinocytosis, and by tetrandrine (1.2 µM; Fig. 7A). As shown in Fig. 7B, fluphenazine and pimozide inhibited Ebola VLP entry with IC_{50} values of 1.3 µM (n_H = 1.7) and 3.6 µM (n_H = 2.8), respectively. Raloxifene, clomiphene and a third SERM, tamoxifen, also inhibited entry with IC_{50} values of 0.61 µM (n_H = 1.1, 0.32 µM (n_H = 1.1) and 0.21 µM (n_H = 0.82), respectively. Enhanced potency of SERMs relative to dopamine receptor antagonists in blocking VLP entry matches that for inhibition of TPC2 currents (Fig. 6).

Discussion

TPCs are channels of physiological, and increasingly, patho-physiological importance [19]. However, their pharmacology is poorly defined and there are currently no approved drugs to target them. To begin to fill this gap, we performed a virtual structure-based screen using a database of approved drugs and the pore region of TPC2 (Fig. 1). Key to our strategy was i) the availability of structural information for mammalian TPCs, ii) the finding that TPCs are novel host factors for EBOV entry and iii) repurposing screens initiated in the wake of the 2014 Ebola epidemic, which yielded a number of approved drugs as novel EBOV entry inhibitors. To prioritise hits, cross-referencing the latter 'wet' data with our 'dry' modelling highlighted drugs targeting dopamine and estrogen receptors (Fig. 2). These drugs demonstrably inhibited TPCs in three independent assays (Figs. 3,5,6), and we correlated their potency with inhibiting Ebola VLP entry (Fig. 7). Single channel analyses confirmed an action of these drugs on the TPC2 pore (Fig 5).

Results from the enrichment analysis of our virtual screen identified a number of drugs targeting distinct G-protein coupled receptors (Fig. 1D). Notably, a high throughput screen for drugs that block EBOV and Marburg virus (both filoviruses) infection also highlighted numerous drugs targeting G-protein coupled receptors [62]. Common drug classes in that screen and ours include those against 5HT, muscarinic and histamine receptors. This further links TPCs to EBOV infection. We focussed our functional analyses on dopamine receptor antagonist and SERMs based on our cross-referencing strategy (Fig. 2). But these compounds represent only a fraction of our top 200 hits. Thus, our screen offers considerable scope for identifying additional TPC blockers in the future.

The dopamine receptor drugs identified here as TPC blockers included several phenothiazines (fluphenazine, trifluoperazine, prochlorperazine and thioridazine) that are used as anti-psychotics (Fig. 2). Our data is consistent with a recent screening campaign published while this work was in progress, which also identified phenothiazines as inhibitors of NAADP-induced Ca^{2+} release from sea urchin egg homogenates [63]. Indeed, the IC_{50} values for fluphenazine, 42µM (Fig. 3B) and ~11 µM [63], are comparable. This congruence highlights the power of our *in silico* strategy for drug identification which, together with our electrophysiological analyses, points mechanistically to drug action on the TPC pore. We also identified the structurally distinct dopamine receptor drug, pimozide, a diphenylbutylpiperidine. As well as targeting the dopamine receptor, pimozide also targets voltage-gated Ca^{2+} channels [64]. The common action of pimozide on TPCs and voltage-gated Ca^{2+} channels likely reflects an evolutionary kindred between these two members of the voltage-gated ion channel superfamily [24]. Although voltage-gated Ca^{2+} channels have been implicated in viral entry [65], their functional absence in non-excitable cells (such as HeLa cells used in this study) points to TPCs as the likely targets.

Our analyses identifying drugs targeting estrogen receptors as additional TPC blockers converged on first (clomiphene, tamoxifen, toremifene), second (raloxifene) and third (bazedoxifene) generation SERMs (Fig. 2). These drugs act as estrogen receptor agonists or antagonists, depending on the tissue, and are used for treating breast cancer and osteoporosis [66]. Off-target effects of these drugs are more than likely related to well-known rapid non-genomic actions of estrogen [67]. Indeed, inhibition of both viral entry and TPC channel activity by sub-micromolar concentrations of raloxifene is striking. Additional effects of SERMs such as destabilisation of either the EBOV glycoprotein [68] or of the lysosomal membranes due to their cationic amphiphilic nature [69] are possible. Nevertheless, both dopamine receptor antagonists and SERMs emerge as novel TPC blockers and provide independent scaffolds for small molecule development.

Estrogen receptor drugs appear more potent in blocking TPC activity (Fig. 6) and Ebola VLP entry (Fig. 7) than dopamine receptor drugs. This correlation points to a common mechanism of action (Fig. 6-7). The half maximal inhibitory concentrations by raloxifene were similar but fluphenazine was more effective at inhibiting VLP entry (Fig. 7) than blocking the channel (Fig. 6). This could reflect additional effects of fluphenazine underlying entry inhibition or the very different conditions under which the two assays were performed (acute drug treatment versus pre-incubation; broken versus intact cells). One other notable difference was the relative poor potency of the drugs in blocking Ca^{2+} signals in egg homogenates (Fig. 3) compared to lysosomal currents (Fig. 6). Again, this could relate to the way in which drugs were administered or the activating ligand. Alternatively, this could point to species differences in drug block. Nevertheless, our study suggests that TPCs may be the target for a number of EBOV entry inhibitors described previously for which mechanistic information was lacking. How TPCs promote EBOV entry is unclear at present. A recent study provided evidence that TPCs may also regulate entry of the MERS corona virus [70]. Pharmacological inhibition with tetrandrine analogues or molecular knockdown of TPCs was shown to reduce Furin activity. This protease activity is required for priming of the envelope protein [71]. Thus, compromised activity upon TPC blockade could underlie reduced MERS corona virus entry. Such a mechanism is unlikely to regulate entry of EBOV because it is processed by endo-lysosomal cathepsins [72]. Moreover, entry of pre-cleaved EBOV is also blocked by tetrandrine [20] suggesting that TPCs act at a step distal to proteolytic processing. Clearly, further work is required to understand the mechanisms of TPC involvement in EBOV entry.

Although cellular studies repeatedly link TPCs to NAADP-mediated Ca^{2+} signalling, electrophysiological analyses of TPCs are less congruent with some studies failing to demonstrate appreciable Ca^{2+} permeability or NAADP activation [39, 73]. Our previous whole cell recordings and single channel analyses demonstrated robust activation of Ca^{2+} and Cs^{+} currents in response to NAADP [32]. Here, we used Na^{+} as the major permeant ion. Comparing single channel conductances in this study (87 pS, Fig. 4) with those for Ca^{2+} (40 pS) and Cs^{+} (128 pS) reported previously [32] points strongly to TPC2 as a non-selective cation channel under these experimental conditions. This conclusion concurs with bilayer studies of TPC2 [74, 75] and electrophysiological analyses of endogenous NAADP-activated TPC2 currents recorded from enlarged vacuoles (Na:Ca permeability ratio close to unity) [76]. TPCs interact with many other proteins [16] some of which likely act to effect and modify gating. Loss of accessory factors might well explain NAADP insensitivity in some studies. Indeed, such loss might also affect the ion selectivity of TPCs as accessory proteins are known to dictate the ion selectivity of other channels such as Orai [77] and MCU [78].

Our single channel analyses provide evidence that the drugs target the pore region of TPCs (Fig. 5). The reduction in open time (~ two-fold) was modest relative to the reduction in open probability (~ 10-fold) pointing to an open channel block mechanism. This is compatible with effects produced by inhibitors known to interact directly with the pore of other channels [79-81]. Of note, phenothiazines have long been known to antagonize calmodulin [82] and previous studies with trifluoperazine have suggested a role for calmodulin in NAADP-mediated Ca^{2+} signalling [83]. Our data, with fluphenazine at least, suggests an additional more direct action of phenothiazines on TPCs likely unrelated to calmodulin (Fig. 5). Clearly, further structure-function analyses is warranted.

In contrast to fluphenazine and raloxifene, Ned-19 did not affect open time (Fig. 5). It thus effectively acts as a gating modifier by reducing the overall frequency of channel openings through directly or indirectly influencing channel regions distal to the pore. Thus, our

analyses uncover fundamentally distinct mechanisms for channel inhibition by the drugs and Ned-19. The lack of effect of Ned-19 (and also NAADP; Fig. 4) on open time support the notion that they act more remotely through associated NAADP-binding proteins. [38]. Uncertainty about the number of channels as well as the limited number of events in patches with low activity prevented us from performing close time distribution analysis upon channel inhibition. But further analysis is warranted not least due to the presence of a multiple closed times (Fig. 4F) which could reflect desensitized states.

In sum, we have identified approved drugs as TPC blockers. We used a novel strategy that affirmed the role of TPCs in EBOV entry and which should significantly aid in expanding the pharmacology of this ubiquitous class of endo-lysosomal ion channels.

Acknowledgments.

This work was supported by PhD studentships from the BBSRC (to CJP and KV), IDB-Cambridge Trust (to XC) and Parkinson's UK (to EY; grant H-1202). MMaz and MMar are supported by UK Medical Research Council funding to the MRC-UCL LMCB University Unit (MC_UU_12018/1). BSK and SP were supported by BBSRC grant BB/N01524X/1. TR was supported by a fellowship and research grant from the Royal Society. We thank Steve Bolsover for useful discussion and Adolfo Garcia Sastre for the gift of plasmids.

[1] G.C. Churchill, Y. Okada, J.M. Thomas, A.A. Genazzani, S. Patel, A. Galione, NAADP mobilizes Ca^{2+} from reserve granules, lysosome-related organelles, in sea urchin eggs, Cell, 111 (2002) 703-708.
[2] H.C. Lee, NAADP-mediated calcium signaling, J. Biol. Chem, 280(40) (2005) 33693-33696.
[3] S. Patel, R. Docampo, Acidic calcium stores open for business: expanding the potential for intracellular Ca^{2+} signaling., Trends Cell Biol, 20 (2010) 277-286.
[4] A.J. Morgan, F.M. Platt, E. Lloyd-Evans, A. Galione, Molecular mechanisms of endolysosomal Ca^{2+} signalling in health and disease, Biochem. J, 439 (2011) 349-374.
[5] S. Patel, X. Cai, Evolution of acid Ca^{2+} stores and their resident Ca^{2+}-permeable channels, Cell Calcium, 57 (2015) 222-230.
[6] P.J. Calcraft, M. Ruas, Z. Pan, X. Cheng, A. Arredouani, X. Hao, J. Tang, K. Rietdorf, L. Teboul, K.T. Chuang, P. Lin, R. Xiao, C. Wang, Y. Zhu, Y. Lin, C.N. Wyatt, J. Parrington, J. Ma, A.M. Evans, A. Galione, M.X. Zhu, NAADP mobilizes calcium from acidic organelles through two-pore channels, Nature, 459 (2009) 596-600.
[7] E. Brailoiu, D. Churamani, X. Cai, M.G. Schrlau, G.C. Brailoiu, X. Gao, R. Hooper, M.J. Boulware, N.J. Dun, J.S. Marchant, S. Patel, Essential requirement for two-pore channel 1 in NAADP-mediated calcium signaling, J. Cell Biol, 186 (2009) 201-209.
[8] X. Zong, M. Schieder, H. Cuny, S. Fenske, C. Gruner, K. Rotzer, O. Griesbeck, H. Harz, M. Biel, C. Wahl-Schott, The two-pore channel TPCN2 mediates NAADP-dependent Ca^{2+}-release from lysosomal stores, Pflugers Arch, 458 (2009) 891-899.
[9] S. Patel, Function and dysfunction of two-pore channels, Sci. Signal, 8 (2015) re7.
[10] J.S. Marchant, S. Patel, Two-pore channels at the intersection of endolysosomal membrane traffic., Biochemical Society Transactions, 43 (2015) 434-441.
[11] C. Grimm, C.C. Chen, C. Wahl-Schott, M. Biel, Two-Pore Channels: Catalyzers of Endolysosomal Transport and Function, Front Pharmacol, 8 (2017) 45.
[12] L.N. Hockey, B.S. Kilpatrick, E.R. Eden, Y. Lin-Moshier, G.C. Brailoiu, E. Brailoiu, C. Futter, A.H. Schapira, J.S. Marchant, S. Patel, Dysregulation of lysosomal morphology by pathogenic LRRK2 is corrected by TPC2 inhibition, J. Cell Sci, 128 (2015) 232-238.
[13] M. Ruas, K. Rietdorf, A. Arredouani, L.C. Davis, E. Lloyd-Evans, H. Koegel, T.M. Funnell, A.J. Morgan, J.A. Ward, K. Watanabe, X. Cheng, G.C. Churchill, M.X. Zhu, F.M. Platt, G.M. Wessel, J. Parrington, A. Galione, Purified TPC isoforms form NAADP receptors with distinct roles for Ca^{2+} Signaling and endolysosomal trafficking, Curr. Biol, 20 (2010) 703-709.
[14] C. Grimm, L.M. Holdt, C.C. Chen, S. Hassan, C. Muller, S. Jors, H. Cuny, S. Kissing, B. Schroder, E. Butz, B. Northoff, J. Castonguay, C.A. Luber, M. Moser, S. Spahn, R. Lullmann-Rauch, C. Fendel, N. Klugbauer, O. Griesbeck, A. Haas, M. Mann, F. Bracher, D. Teupser, P. Saftig, M. Biel, C. Wahl-Schott, High susceptibility to fatty liver disease in two-pore channel 2-deficient mice, Nat. Commun, 5 (2014) 4699.
[15] M. Ruas, K.T. Chuang, L.C. Davis, A. Al-Douri, P.W. Tynan, R. Tunn, L. Teboul, A. Galione, J. Parrington, TPC1 has two variant isoforms and their removal has different effects on endo-lysosomal functions compared to loss of TPC2, Mol. Cell Biol, 34 (2014) 3981-3992.
[16] Y. Lin-Moshier, M.V. Keebler, R. Hooper, M.J. Boulware, X. Liu, D. Churamani, M.E. Abood, T.F. Walseth, E. Brailoiu, S. Patel, J.S. Marchant, The two-pore channel (TPC) interactome unmasks isoform-specific roles for TPCs in endolysosomal morphology and cell pigmentation, PNAS, 111 (2014) 13087-13092.
[17] O.N. Nguyen, C. Grimm, L.S. Schneider, Y.K. Chao, C. Atzberger, K. Bartel, A. Watermann, M. Ulrich, D. Mayr, C. Wahl-Schott, M. Biel, A.M. Vollmar, Two-Pore Channel Function Is Crucial for the Migration of Invasive Cancer Cells, Cancer Res, 77 (2017) 1427-1438.
[18] B.S. Kilpatrick, E.R. Eden, L.N. Hockey, E. Yates, C.E. Futter, S. Patel, An Endosomal NAADP-Sensitive Two-Pore Ca2+ Channel Regulates ER-Endosome Membrane Contact Sites to Control Growth Factor Signaling, Cell Rep, 18 (2017) 1636-1645.
[19] S. Patel, B.S. Kilpatrick, Two-pore channels and disease, Biochimica et biophysica acta, (2018).

[20] Y. Sakurai, A.A. Kolokolstov, C.C. Chen, M.W. Tidwell, W.E. Bauta, N. Klugbauer, C. Grimm, C. Wahl-Schott, M. Biel, R.A. Davey, Two-pore channels control Ebola virus host cell entry and are drug targets for disease treatment, Science, 347 (2015) 6225.
[21] M. Cote, J. Misasi, T. Ren, A. Bruchez, K. Lee, C.M. Filone, L. Hensley, Q. Li, D. Ory, K. Chandran, J. Cunningham, Small molecule inhibitors reveal Niemann-Pick C1 is essential for Ebola virus infection, Nature, 477 (2011) 344-348.
[22] J.A. Simmons, R.S. D'Souza, M. Ruas, A. Galione, J.E. Casanova, J.M. White, Ebolavirus Glycoprotein Directs Fusion through NPC1+ Endolysosomes, Journal of virology, 90 (2016) 605-610.
[23] D. Churamani, R. Hooper, E. Brailoiu, S. Patel, Domain assembly of NAADP-gated two-pore channels, Biochem. J, 441 (2012) 317-323.
[24] T. Rahman, X. Cai, G.C. Brailoiu, M.E. Abood, E. Brailoiu, S. Patel, Two-pore channels provide insight into the evolution of voltage-gated Ca^{2+} and Na^{+} channels, Sci. Signal, 7 (2014) ra109.
[25] C.J. Penny, T. Rahman, A. Sula, A.J. Miles, B.A. Wallace, S. Patel, Isolated pores dissected from human two-pore channel 2 are functional, Sci. Rep, 6 (2016) 38426.
[26] J. Guo, W. Zeng, Q. Chen, C. Lee, L. Chen, Y. Yang, C. Cang, D. Ren, Y. Jiang, Structure of the voltage-gated two-pore channel TPC1 from Arabidopsis thaliana, Nature, 531 (2016) 196-201.
[27] A.F. Kintzer, R.M. Stroud, Structure, inhibition and regulation of two-pore channel TPC1 from Arabidopsis thaliana, Nature, 531 (2016) 258-264.
[28] S. Patel, C.J. Penny, T. Rahman, Two-pore Channels Enter the Atomic Era. Structure of plant TPC revealed., Trends Biochem. Sci, 41 (2016) 475-477.
[29] J. She, J. Guo, Q. Chen, W. Zeng, Y. Jiang, X.C. Bai, Structural insights into the voltage and phospholipid activation of the mammalian TPC1 channel, Nature, 556 (2018) 130-134.
[30] S. Patel, Two-pore channels open up, Nature, 556 (2018) 38-40.
[31] X. Cai, S. Patel, Degeneration of an intracellular ion channel in the primate lineage by relaxation of selective constraints, Mol. Biol. Evol, 27 (2010) 2352-2359.
[32] E. Brailoiu, T. Rahman, D. Churamani, D.L. Prole, G.C. Brailoiu, R. Hooper, C.W. Taylor, S. Patel, An NAADP-gated two-pore channel targeted to the plasma membrane uncouples triggering from amplifying Ca^{2+} signals, J. Biol. Chem, 285 (2010) 38511-38516.
[33] J.S. Marchant, S. Patel, Questioning regulation of two-pore channels by NAADP, Messenger, 2 (2013) 113-119.
[34] A.J. Morgan, A. Galione, Two-pore channels (TPCs): Current controversies, BioEssays, 36 (2013) 173-183.
[35] Y. Lin-Moshier, T.F. Walseth, D. Churamani, S.M. Davidson, J.T. Slama, R. Hooper, E. Brailoiu, S. Patel, J.S. Marchant, Photoaffinity labeling of nicotinic acid adenine dinucleotide phosphate (NAADP) targets in mammalian cells, J. Biol. Chem, 287 (2012) 2296-2307.
[36] T.F. Walseth, Y. Lin-Moshier, P. Jain, M. Ruas, J. Parrington, A. Galione, J.S. Marchant, J.T. Slama, Photoaffinity labeling of high affinity nicotinic acid adenine dinucleotide 2'-phosphate (NAADP) proteins in sea urchin egg, J. Biol. Chem, 287 (2012) 2308-2315.
[37] T.F. Walseth, Y. Lin-Moshier, K. Weber, J.S. Marchant, J.T. Slama, A.H. Guse, Nicotinic Acid Adenine Dinucleotide 2'-Phosphate (NAADP) Binding Proteins in T-Lymphocytes, Messenger (Los. Angel.), 1 (2012) 86-94.
[38] J.S. Marchant, Y. Lin-Moshier, T.F. Walseth, S. Patel, The Molecular Basis for Ca^{2+} Signalling by NAADP: Two-Pore Channels in a Complex?, Messenger, 1 (2012) 63-76.
[39] X. Wang, X. Zhang, X.P. Dong, M. Samie, X. Li, X. Cheng, A. Goschka, D. Shen, Y. Zhou, J. Harlow, M.X. Zhu, D.E. Clapham, D. Ren, H. Xu, TPC proteins are phosphoinositide- activated sodium-selective ion channels in endosomes and lysosomes, Cell, 151 (2012) 372-383.
[40] S. Patel, D. Churamani, E. Brailoiu, NAADP-evoked Ca(2+) signals through two-pore channel-1 require arginine residues in the first S4-S5 linker, Cell Calcium, 68 (2017) 1-4.
[41] W. Dammermann, B. Zhang, M. Nebel, C. Cordiglieri, F. Odoardi, T. Kirchberger, N. Kawakami, J. Dowden, F. Schmid, K. Dornmair, M. Hohenegger, A. Flugel, A.H. Guse, B.V. Potter, NAADP-mediated

Ca^{2+} signaling via type 1 ryanodine receptor in T cells revealed by a synthetic NAADP antagonist, Proc. Natl. Acad. Sci. U. S. A, 106 (2009) 10678-10683.
[42] E. Naylor, A. Arredouani, S.R. Vasudevan, A.M. Lewis, R. Parkesh, A. Mizote, D. Rosen, J.M. Thomas, M. Izumi, A. Ganesan, A. Galione, G.C. Churchill, Identification of a chemical probe for NAADP by virtual screening, Nat. Chem. Biol, 5 (2009) 220-226.
[43] A.H. Guse, Linking NAADP to Ion Channel Activity: A Unifying Hypothesis, Sci. Signal, 5 (2012) e18.
[44] I. Pafumi, M. Festa, F. Papacci, L. Lagostena, C. Giunta, V. Gutla, L. Cornara, A. Favia, F. Palombi, F. Gambale, A. Filippini, A. Carpaneto, Naringenin Impairs Two-Pore Channel 2 Activity And Inhibits VEGF-Induced Angiogenesis, Scientific reports, 7 (2017) 5121.
[45] A. Waterhouse, M. Bertoni, S. Bienert, G. Studer, G. Tauriello, R. Gumienny, F.T. Heer, T.A.P. de Beer, C. Rempfer, L. Bordoli, R. Lepore, T. Schwede, SWISS-MODEL: homology modelling of protein structures and complexes, Nucleic Acids Res, 46 (2018) W296-w303.
[46] J. Ko, H. Park, L. Heo, C. Seok, GalaxyWEB server for protein structure prediction and refinement, Nucleic Acids Res, 40 (2012) W294-297.
[47] E. Pihan, L. Colliandre, J.F. Guichou, D. Douguet, e-Drug3D: 3D structure collections dedicated to drug repurposing and fragment-based drug design, Bioinformatics, 28 (2012) 1540-1541.
[48] O. Trott, A.J. Olson, AutoDock Vina: improving the speed and accuracy of docking with a new scoring function, efficient optimization, and multithreading, Journal of computational chemistry, 31 (2010) 455-461.
[49] G.D. Dickinson, S. Patel, Modulation of NAADP receptors by K^+ ions: Evidence for multiple NAADP receptor conformations, BJ, 375 (2003) 805-812.
[50] U.R. Taufiq, A. Skupin, M. Falcke, C.W. Taylor, Clustering of $InsP_3$ receptors by $InsP_3$ retunes their regulation by $InsP_3$ and Ca^{2+}, Nature, 458 (2009) 655-659.
[51] D. Colquhoun, Practical Analysis of Single Channel Records, in: N.B. Standen (Ed.) Microelectrode Techniques: The Plymouth Workshop Handbook, Place Published, 1994.
[52] F. Qin, A. Auerbach, F. Sachs, A direct optimization approach to hidden Markov modeling for single channel kinetics, Biophysical journal, 79 (2000) 1915-1927.
[53] L. Ionescu, K.H. Cheung, H. Vais, D.O. Mak, C. White, J.K. Foskett, Graded recruitment and inactivation of single InsP3 receptor Ca2+-release channels: implications for quantal [corrected] Ca2+release, The Journal of physiology, 573 (2006) 645-662.
[54] A. Jha, M. Ahuja, S. Patel, E. Brailoiu, S. Muallem, Convergent Regulation of the Lysosomal Two-Pore Channel-2 by Mg^{2+}, NAADP, $PI(3,5)P_2$ and Multiple Protein Kinases, EMBO J, 33 (2014) 501-511.
[55] D.M. Tscherne, B. Manicassamy, A. Garcia-Sastre, An enzymatic virus-like particle assay for sensitive detection of virus entry, Journal of virological methods, 163 (2010) 336-343.
[56] B. Manicassamy, L. Rong, Expression of Ebolavirus glycoprotein on the target cells enhances viral entry, Virology journal, 6 (2009) 75.
[57] B. Manicassamy, J. Wang, H. Jiang, L. Rong, Comprehensive analysis of ebola virus GP1 in viral entry, Journal of virology, 79 (2005) 4793-4805.
[58] J. Kouznetsova, W. Sun, C. Martinez-Romero, G. Tawa, P. Shinn, C.Z. Chen, A. Schimmer, P. Sanderson, J.C. McKew, W. Zheng, A. Garcia-Sastre, Identification of 53 compounds that block Ebola virus-like particle entry via a repurposing screen of approved drugs, Emerg. Microbes. Infect, 3 (2014) e84.
[59] L.M. Johansen, L.E. DeWald, C.J. Shoemaker, B.G. Hoffstrom, C.M. Lear-Rooney, A. Stossel, E. Nelson, S.E. Delos, J.A. Simmons, J.M. Grenier, L.T. Pierce, H. Pajouhesh, J. Lehar, L.E. Hensley, P.J. Glass, J.M. White, G.G. Olinger, A screen of approved drugs and molecular probes identifies therapeutics with anti-Ebola virus activity, Sci. Transl. Med, 7 (2015) 290ra289.
[60] A. Galione, K.T. Chuang, T.M. Funnell, L.C. Davis, A.J. Morgan, M. Ruas, J. Parrington, G.C. Churchill, Preparation and use of sea urchin egg homogenates for studying NAADP-mediated Ca^{2+} release, Cold Spring Harb. Protoc, 2014 (2014) 988-992.

[61] S.A. Kirsch, A. Kugemann, A. Carpaneto, R.A. Bockmann, P. Dietrich, Phosphatidylinositol-3,5-bisphosphate lipid-binding-induced activation of the human two-pore channel 2, Cell Mol Life Sci, (2018).
[62] H. Cheng, C.M. Lear-Rooney, L. Johansen, E. Varhegyi, Z.W. Chen, G.G. Olinger, L. Rong, Inhibition of Ebola and Marburg Virus Entry by G Protein-Coupled Receptor Antagonists, Journal of virology, 89 (2015) 9932-9938.
[63] G.S. Gunaratne, M.E. Johns, H.M. Hintz, T.F. Walseth, J.S. Marchant, A screening campaign in sea urchin egg homogenate as a platform for discovering modulators of NAADP-dependent Ca(2+) signaling in human cells, Cell Calcium, 75 (2018) 42-52.
[64] J.J. Enyeart, R.T. Dirksen, V.K. Sharma, D.J. Williford, S.S. Sheu, Antipsychotic pimozide is a potent Ca2+ channel blocker in heart, Molecular pharmacology, 37 (1990) 752-757.
[65] M. Lavanya, C.D. Cuevas, M. Thomas, S. Cherry, S.R. Ross, siRNA screen for genes that affect Junin virus entry uncovers voltage-gated calcium channels as a therapeutic target, Sci. Transl. Med, 5 (2013) 204ra131.
[66] M. Dutertre, C.L. Smith, Molecular mechanisms of selective estrogen receptor modulator (SERM) action, The Journal of pharmacology and experimental therapeutics, 295 (2000) 431-437.
[67] L.M. Kow, D.W. Pfaff, Rapid estrogen actions on ion channels: A survey in search for mechanisms, Steroids, 111 (2016) 46-53.
[68] Y. Zhao, J. Ren, K. Harlos, D.M. Jones, A. Zeltina, T.A. Bowden, S. Padilla-Parra, E.E. Fry, D.I. Stuart, Toremifene interacts with and destabilizes the Ebola virus glycoprotein, Nature, 535 (2016) 169-172.
[69] C.J. Shoemaker, K.L. Schornberg, S.E. Delos, C. Scully, H. Pajouhesh, G.G. Olinger, L.M. Johansen, J.M. White, Multiple cationic amphiphiles induce a Niemann-Pick C phenotype and inhibit Ebola virus entry and infection, PloS one, 8 (2013) e56265.
[70] G.S. Gunaratne, Y. Yang, F. Li, T.F. Walseth, J.S. Marchant, NAADP-dependent Ca(2+) signaling regulates Middle East respiratory syndrome-coronavirus pseudovirus translocation through the endolysosomal system, Cell Calcium, 75 (2018) 30-41.
[71] J.K. Millet, G.R. Whittaker, Host cell entry of Middle East respiratory syndrome coronavirus after two-step, furin-mediated activation of the spike protein, Proceedings of the National Academy of Sciences of the United States of America, 111 (2014) 15214-15219.
[72] K. Chandran, N.J. Sullivan, U. Felbor, S.P. Whelan, J.M. Cunningham, Endosomal proteolysis of the Ebola virus glycoprotein is necessary for infection, Science, 308 (2005) 1643-1645.
[73] J. Guo, W. Zeng, Y. Jiang, Tuning the ion selectivity of two-pore channels, Proceedings of the National Academy of Sciences of the United States of America, 114 (2017) 1009-1014.
[74] S.J. Pitt, T. Funnell, M. Sitsapesan, E. Venturi, K. Rietdorf, M. Ruas, A. Ganesan, R. Gosain, G.C. Churchill, M.X. Zhu, J. Parrington, A. Galione, R. Sitsapesan, TPC2 is a novel NAADP-sensitive Ca^{2+}-release channel, operating as a dual sensor of luminal pH and Ca^{2+}, J. Biol. Chem, 285 (2010) 24925-24932.
[75] C.S. Lee, B.C. Tong, C.W. Cheng, H.C. Hung, K.H. Cheung, Characterization of Two-Pore Channel 2 by Nuclear Membrane Electrophysiology, Scientific reports, 6 (2016) 20282.
[76] M. Ruas, L.C. Davis, C.C. Chen, A.J. Morgan, K.T. Chuang, T.F. Walseth, C. Grimm, C. Garnham, T. Powell, N. Platt, F.M. Platt, M. Biel, C. Wahl-Schott, J. Parrington, A. Galione, Expression of Ca^{2+}-permeable two-pore channels rescues NAADP signalling in TPC-deficient cells, EMBO J, 34 (2015) 1743-1758.
[77] P. Li, Y. Miao, A. Dani, M. Vig, alpha-SNAP regulates dynamic, on-site assembly and calcium selectivity of Orai1 channels, Molecular biology of the cell, 27 (2016) 2542-2553.
[78] K.J. Kamer, Y. Sancak, Y. Fomina, J.D. Meisel, D. Chaudhuri, Z. Grabarek, V.K. Mootha, MICU1 imparts the mitochondrial uniporter with the ability to discriminate between Ca(2+) and Mn(2), Proceedings of the National Academy of Sciences of the United States of America, (2018).

[79] M.J. Barber, D.J. Wendt, C.F. Starmer, A.O. Grant, Blockade of cardiac sodium channels. Competition between the permeant ion and antiarrhythmic drugs, The Journal of clinical investigation, 90 (1992) 368-381.
[80] V. Avdonin, E.F. Shibata, T. Hoshi, Dihydropyridine action on voltage-dependent potassium channels expressed in Xenopus oocytes, The Journal of general physiology, 109 (1997) 169-180.
[81] A.A. Harper, L. Catacuzzeno, C. Trequattrini, A. Petris, F. Franciolini, Verapamil block of large-conductance Ca-activated K channels in rat aortic myocytes, The Journal of membrane biology, 179 (2001) 103-111.
[82] R.M. Levin, B. Weiss, Binding of trifluoperazine to the calcium-dependent activator of cyclic nucleotide phosphodiesterase, Molecular pharmacology, 13 (1977) 690-697.
[83] A.A. Genazzani, M. Mezna, D.M. Dickey, F. Michelangeli, T.F. Walseth, A. Galione, Pharmacological properties of the Ca^{2+}-release mechanism sensitive to NAADP in the sea urchin egg., Br. J. Pharmacol, 121 (1997) 1489-1495.

Figure 1 A structure-based virtual screen of approved drugs based on the TPC2 pore.

A, Structural model of human TPC2 viewed from the cytosolic face. The pore region is highlighted by the dashed box.

B, Results of a virtual screen of the e-Drugs3D database against the pore region of TPC2. The top 200 drugs are marked by the shaded region.

C, Plots showing the rank of individual drugs from the virtual screen targeting voltage-gated Ca^{2+} and Na^{+} channels. The horizontal lines represent the mean. Nicardipine (rank #154) and diltiazem (rank #247) are highlighted*.

D, Enrichment analysis of drug classes within the top 200 hits. G-protein coupled receptors are highlighted*.

Figure 2 Identification of drugs targeting dopamine and estrogen receptors as putative TPC2 inhibitors.

A, Venn diagram depicting the relationship between approved drugs identified as Ebola virus entry inhibitors in independent high through put screens by Kouznetsova [58] and Johansen [59] et al.

B, Venn diagram depicting the relationships between the entry inhibitors identified in A with the e-Drugs3D database used for the TPC virtual screen.

C, Venn diagram depicting the relationship between entry inhibitors present in the e-drugs3-D database and the top 200 hits from the TPC virtual screen.

D, Prioritised set of 14 drugs identified from **C** listing their rank in the TPC virtual screen, their reported IC_{50} values for inhibiting virus entry (from Kouznetsova [58] and/or [a]Johansen [59] et al.) and their primary target (annotated in e-Drugs3D).

Figure 3 Dopamine antagonists and selective estrogen receptor modulators block endogenous NAADP-mediated Ca^{2+} signals.

A, Exemplar Ca^{2+} signals, recorded using Fluo-4 from sea urchin egg homogenates pre-incubated with the indicated drug (100 µM) or DMSO (black traces) for ~ 1 min prior to stimulation with NAADP (1 µM).

B, Concentration-effect relationships for blockade of NAADP responses by the various drugs (n = 3). Data are normalised to the NAADP response in the presence of DMSO.

C, Summary data quantifying the effect of the drugs (100 µM) on Ca^{2+} response to NAADP versus cyclic ADP-ribose (n = 3). Data are normalised to the NAADP and cyclic ADP-ribose responses in the presence of DMSO.

Figure 4 NAADP stimulates single channel activity of TPC2 rerouted to the plasma membrane.

A, Exemplar single channel recordings from inside-out patches excised from HEK cells expressing plasma membrane-targeted TPC2 in response to the indicated concentrations of NAADP. Na^+ was the charge carrier and the holding potential was +40 mV. *C* denotes the closed state.

B, Summary data quantifying open probability (NP_o; n = 3 – 28).

C, Current-voltage relationships derived from records similar to those shown in **A** (n = 3).

D, Exemplar open and closed time distributions at the indicated NAADP concentration.

E, Summary data quantifying mean open time (n = 3 – 28).

F, Likely gating schemes for TPC2.

Figure 5 Dopamine antagonists and selective estrogen receptor modulators inhibit single channel activity of TPC2 by reducing open time.

A – C, Exemplar single channel records from inside-out patches expressing plasma membrane-targeted TPC2. Patches were sequentially challenged with 100 nM NAADP and either fluphenazine (100 µM; **A**), raloxifene (100 µM; **B**) or Ned-19 (1 µM; **C**). Large vertical deflections are addition artefacts. Red bars indicate the sections of the upper trace in the presence of NAADP before and after drug addition that were expanded in the corresponding lower traces.

D – F, Exemplar open time distributions from records similar to A – C in the presence of the indicated drug.

G, Summary data quantifying open probability, mean closed time and unitary conductance for TPC2 activity in response to 100 nM NAADP in the absence (n = 10) and presence of the indicated drug (n = 3 – 4).

Figure 6 Dopamine antagonists and selective estrogen receptor modulators inhibit lysosomal TPC2 currents

A, Exemplar currents recorded from enlarged lysosomes isolated from HEK cells expressing lysosome-targeted TPC2 in response to $PI(3,5)P_2$ (1 µM). The holding potentials were +100 mV (upper traces) and -100 mV (lower traces). Lysosomes were challenged with fluphenazine (Flu.) and raloxifene (Ral.) at the concentrations and for the times indicated.

B, Concentration-effect relationships for blockade of $PI(3,5)P_2$ currents by the drugs (n = 2). Data are normalised to the $PI(3,5)P_2$ response in the absence of the drugs.

Figure 7 Dopamine antagonists and selective estrogen receptor modulators inhibit entry of Ebola virus-like particles.

A, Infection of HeLa cells with Ebola virus-like particles in the absence and presence of EIPA (11.1 µM; n = 3) or tetrandrine (1.2 µM; n = 4).

B, Concentration-effect relationships for blockade of virus-like particle entry by the indicated dopamine antagonist (squares) or SERMs (circles). n = 3 – 4.

Highlights

Identification of approved drugs as TPC2 pore blockers through virtual screening.

Prioritisation of drugs that inhibit Ebola virus entry.

Blockade of endogenous and recombinant TPC2 channel activity by select drugs.

Similar potency for inhibition channel activity and Ebola virus entry.

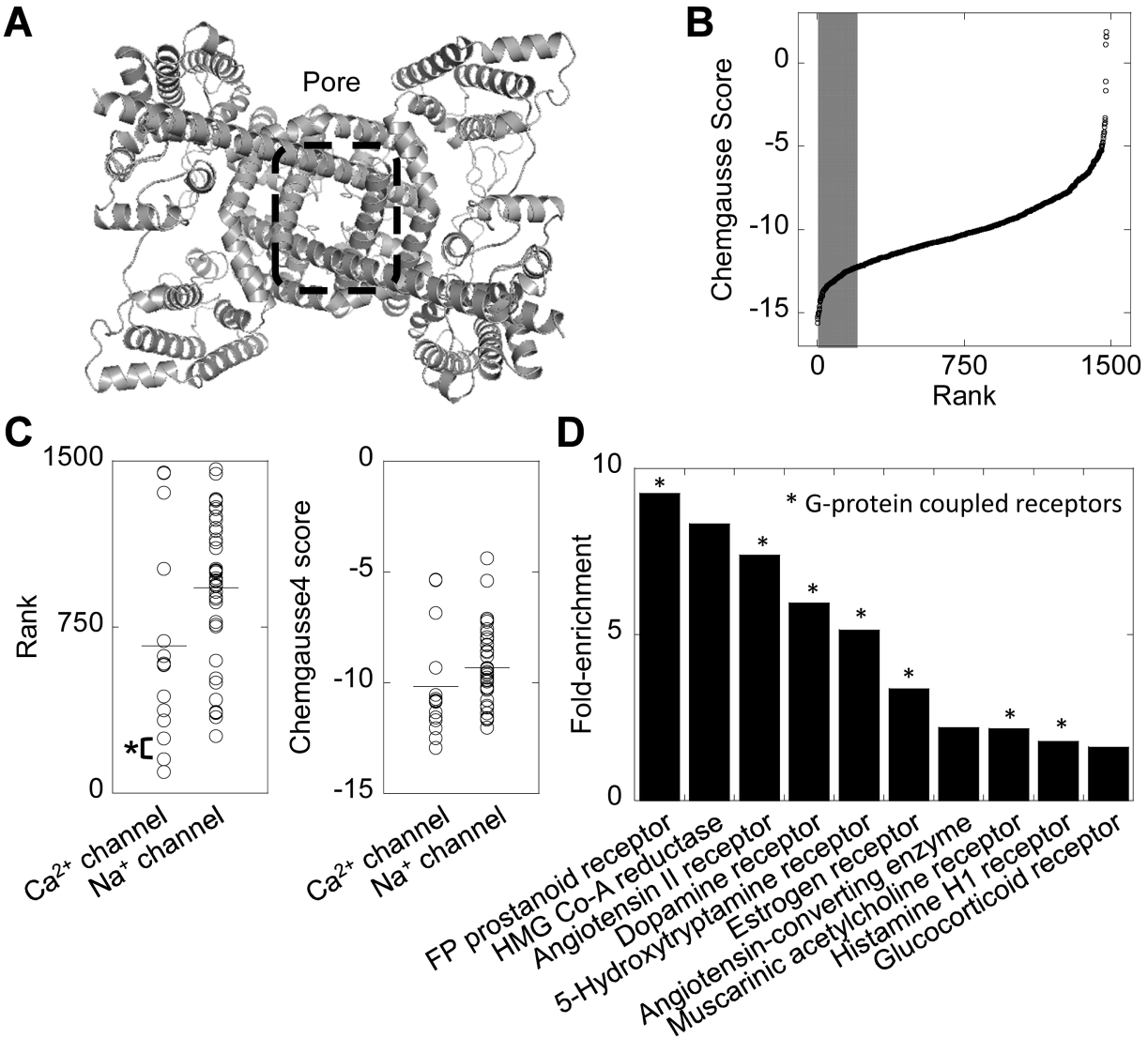
A
Pore
B
Chemgausse Score
0
-5
-10
-15
0
750
1500
Rank
C
Rank
1500
750
0
*
Ca2+ channel
Na+ channel
Chemgausse4 score
0
-5
-10
-15
Ca2+ channel
Na+ channel
D
Fold-enrichment
10
5
0
* G-protein coupled receptors
FP prostanoid receptor
HMG Co-A reductase
Angiotensin II receptor
Dopamine receptor
5-Hydroxytryptamine receptor
Estrogen receptor
Angiotensin-converting enzyme
Muscarinic acetylcholine receptor
Histamine H1 receptor
Glucocorticoid receptor

Figure 1

A

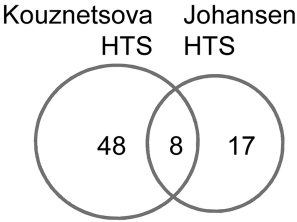

B

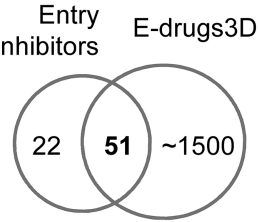

C

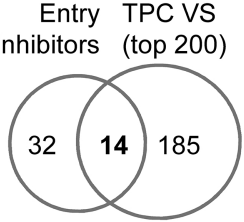

D

Drug	TPC VS (Rank)	Ebola HTS (IC_{50}, μM)	Target
Amodiaquine	58	4.43	-
Clomiphene	60	1.72, 2.42 [a]	Estrogen receptor
Piperacetazine	80	9.68, 12.3 [a]	-
Bazedoxifene	82	3.43	Estrogen receptor
Fluphenazine	95	5.54 [a]	Dopamine receptor
Bepridil	97	5.08 [a]	Ca^{2+} channel
Pimozide	100	3.12 [a]	Dopamine receptor
Trifluoperazine	106	4.48	Dopamine receptor
Raloxifene	109	1.84	Estrogen receptor
Tamoxifen	113	0.734	Estrogen receptor
Prochlorperazine	115	5.96 [a]	Dopamine receptor
Simvastatin	119	44.6 [a]	HMG-CoA reductase
Thioridazine	163	6.24 [a]	Dopamine receptor
Toremifene	176	0.566, 0.16 [a]	Estrogen receptor

Figure 2

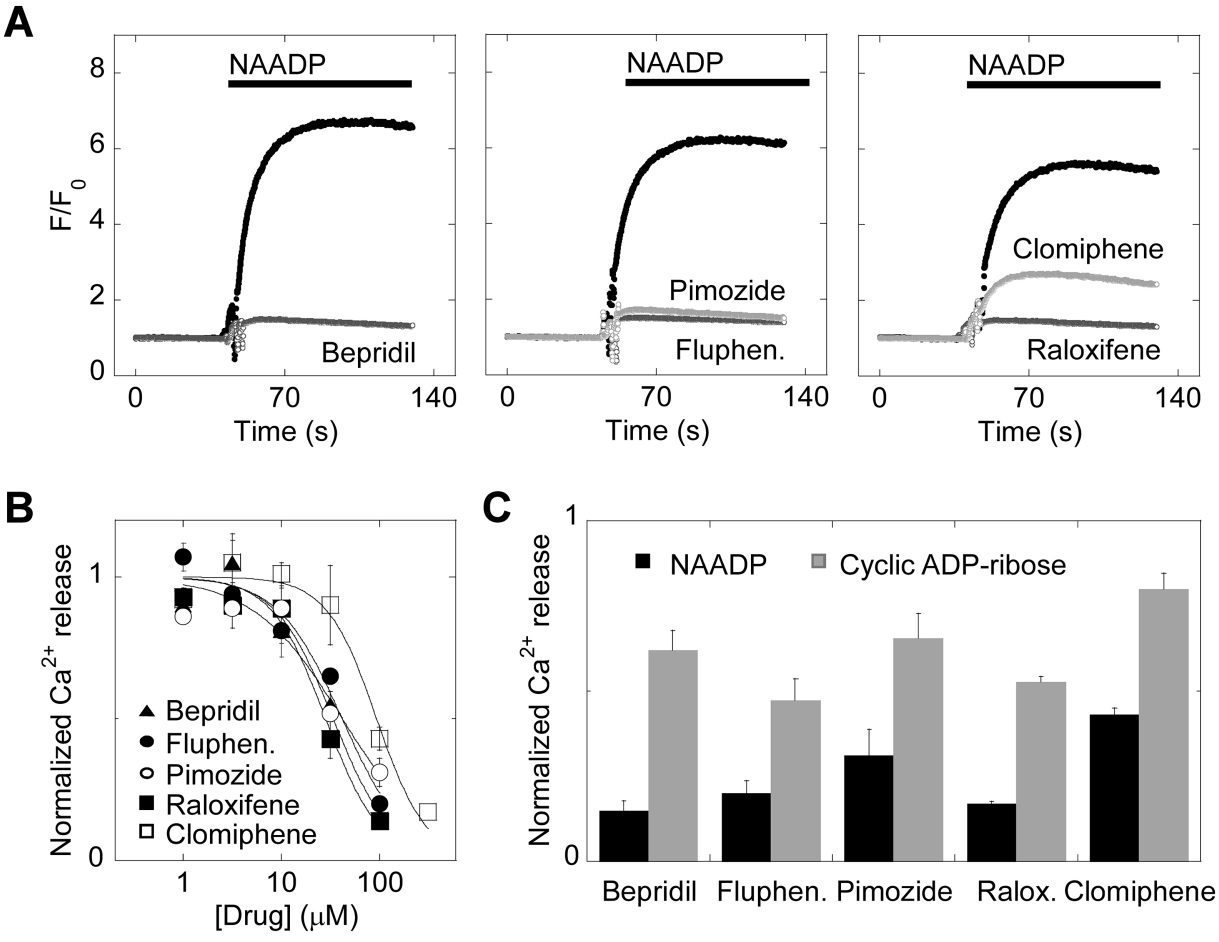
A
NAADP
NAADP
NAADP
F/F0
Bepridil
Pimozide
Fluphen.
Clomiphene
Raloxifene
Time (s)
Time (s)
Time (s)
B
Normalized Ca2+ release
Bepridil
Fluphen.
Pimozide
Raloxifene
Clomiphene
[Drug] (μM)
C
Normalized Ca2+ release
NAADP
Cyclic ADP-ribose
Bepridil
Fluphen.
Pimozide
Ralox.
Clomiphene

Figure 3

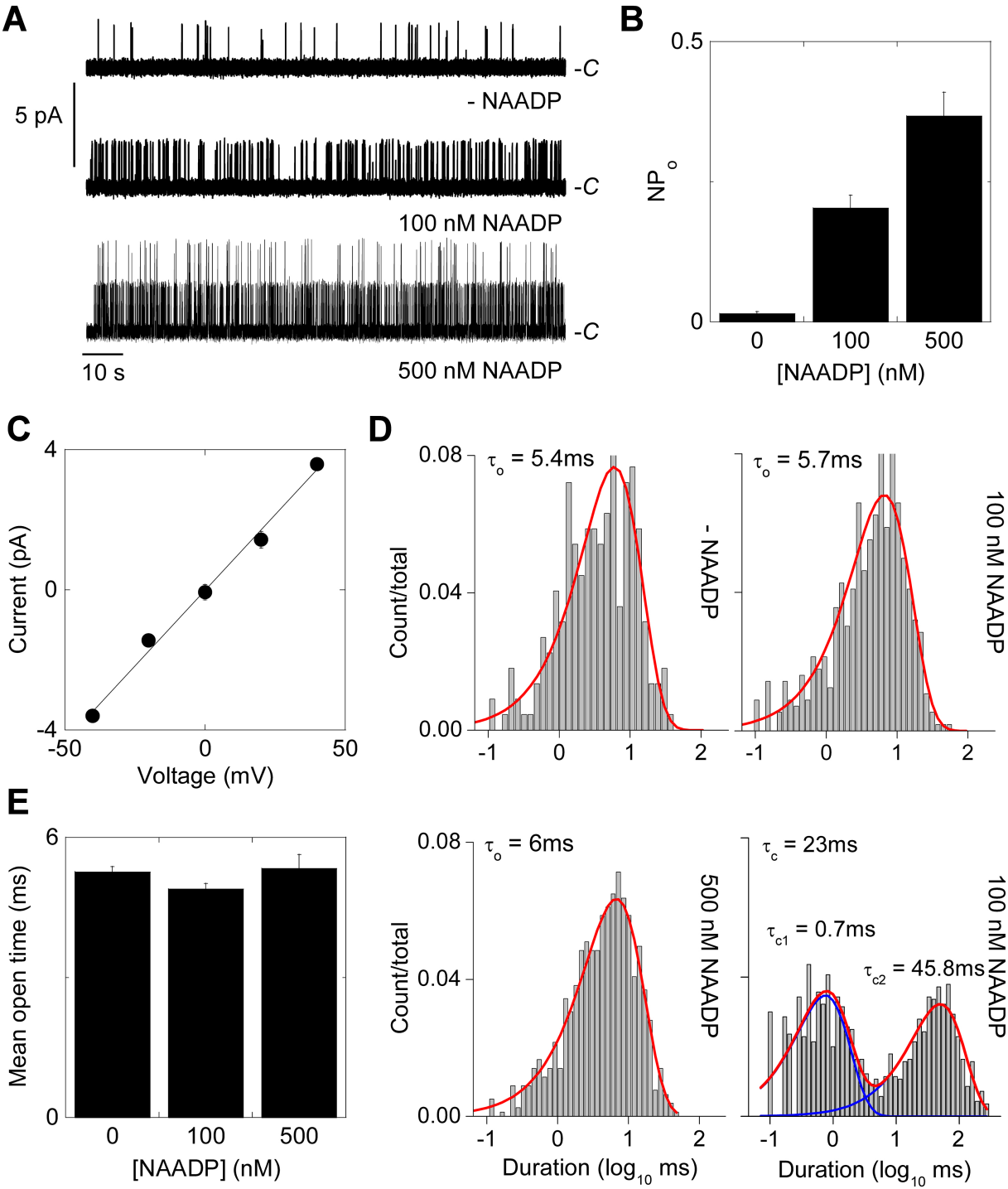
A
5 pA
-C
- NAADP
-C
100 nM NAADP
-C
10 s
500 nM NAADP
B
0.5
0
NP o
0
100
500
[NAADP] (nM)
C
4
0
-4
Current (pA)
-50
0
50
Voltage (mV)
D
0.08
0.04
0.00
Count/total
τo = 5.4ms
- NAADP
τo = 5.7ms
100 nM NAADP
-1
0
1
2
E
6
0
Mean open time (ms)
0
100
500
[NAADP] (nM)
0.08
0.04
0.00
Count/total
τo = 6ms
500 nM NAADP
Duration (log10 ms)
τc = 23ms
τc1 = 0.7ms
τc2 = 45.8ms
100 nM NAADP
Duration (log10 ms)
F
C1
k12
k21
C2
β
α
O
C1
k10
k01
O
β
α
C2

Figure 4

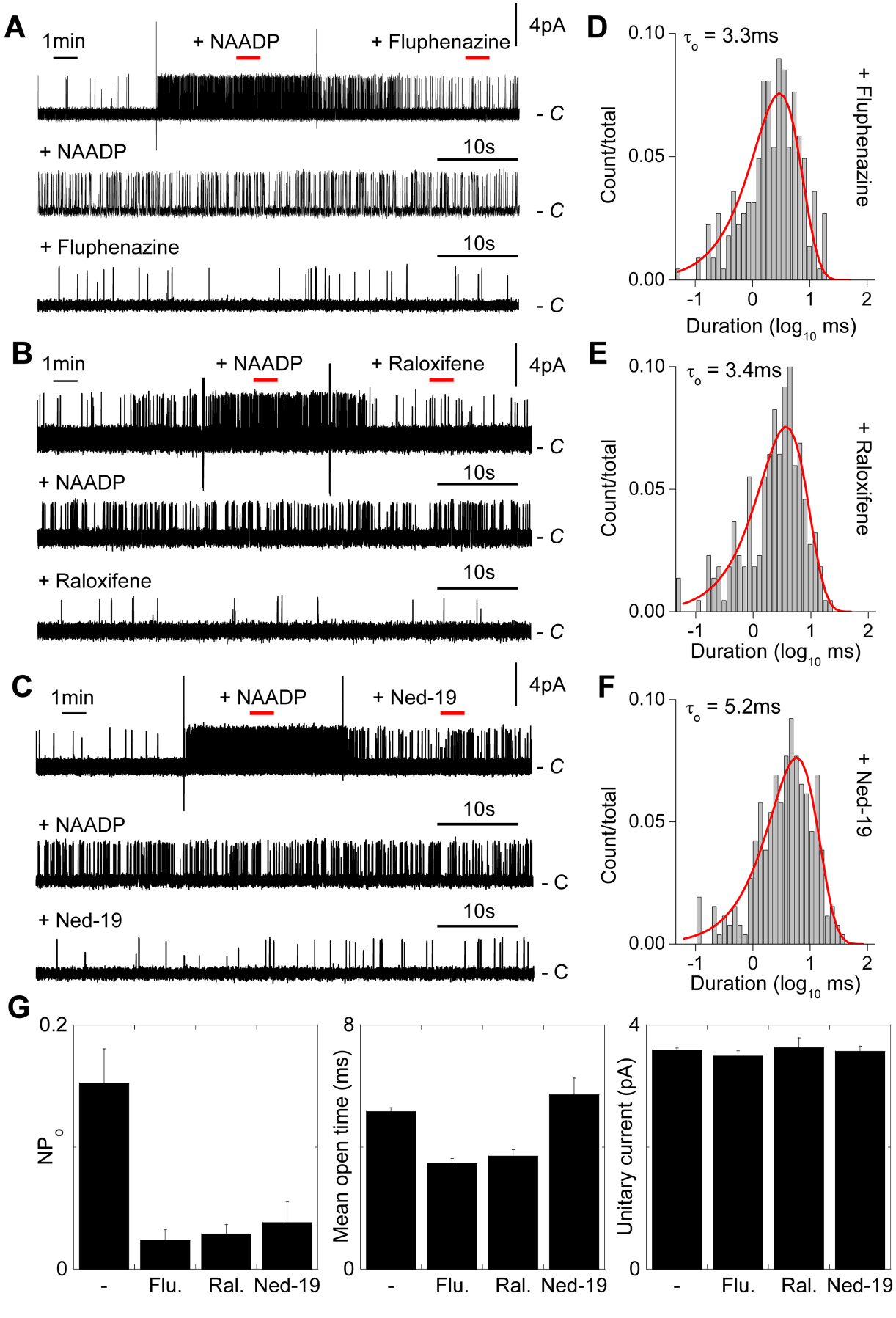
A
1min
+ NAADP
+ Fluphenazine
4pA
- C
+ NAADP
10s
- C
+ Fluphenazine
10s
- C
B
1min
+ NAADP
+ Raloxifene
4pA
- C
+ NAADP
10s
- C
+ Raloxifene
10s
- C
C
1min
+ NAADP
+ Ned-19
4pA
- C
+ NAADP
10s
- C
+ Ned-19
10s
- C
D
τo = 3.3ms
+ Fluphenazine
Count/total
0.10
0.05
0.00
-1
0
1
2
Duration (log10 ms)
E
τo = 3.4ms
+ Raloxifene
Count/total
0.10
0.05
0.00
-1
0
1
2
Duration (log10 ms)
F
τo = 5.2ms
+ Ned-19
Count/total
0.10
0.05
0.00
-1
0
1
2
Duration (log10 ms)
G
NPo
0.2
0
-
Flu.
Ral.
Ned-19
Mean open time (ms)
8
0
-
Flu.
Ral.
Ned-19
Unitary current (pA)
4
0
-
Flu.
Ral.
Ned-19

Figure 5

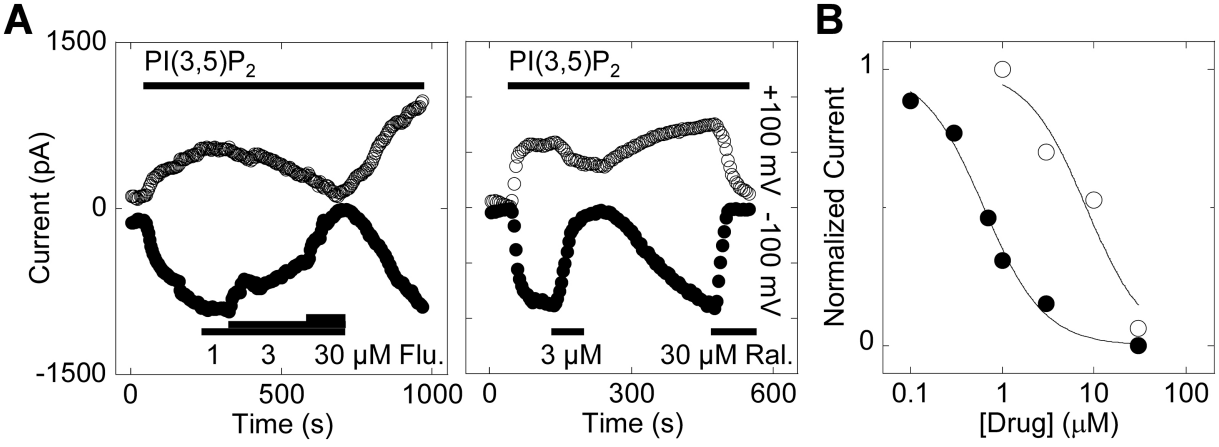
A
1500
0
-1500
Current (pA)
PI(3,5)P2
1
3
30 μM Flu.
0
500
1000
Time (s)
PI(3,5)P2
+100 mV
-100 mV
3 μM
30 μM Ral.
0
300
600
Time (s)
B
1
0
Normalized Current
0.1
1
10
100
[Drug] (μM)

Figure 6

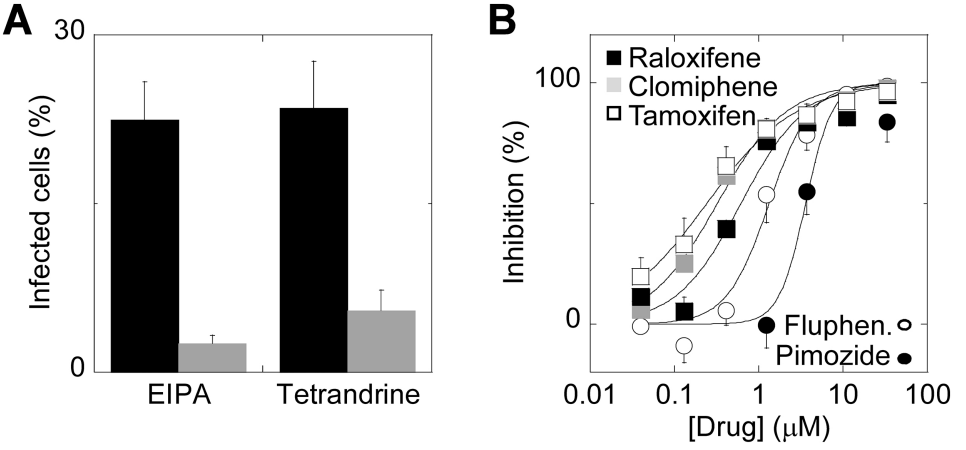
A
30
0
Infected cells (%)
EIPA
Tetrandrine
B
Raloxifene
Clomiphene
Tamoxifen
100
0
Inhibition (%)
Fluphen.
Pimozide
0.01
0.1
1
10
100
[Drug] (μM)

Figure 7

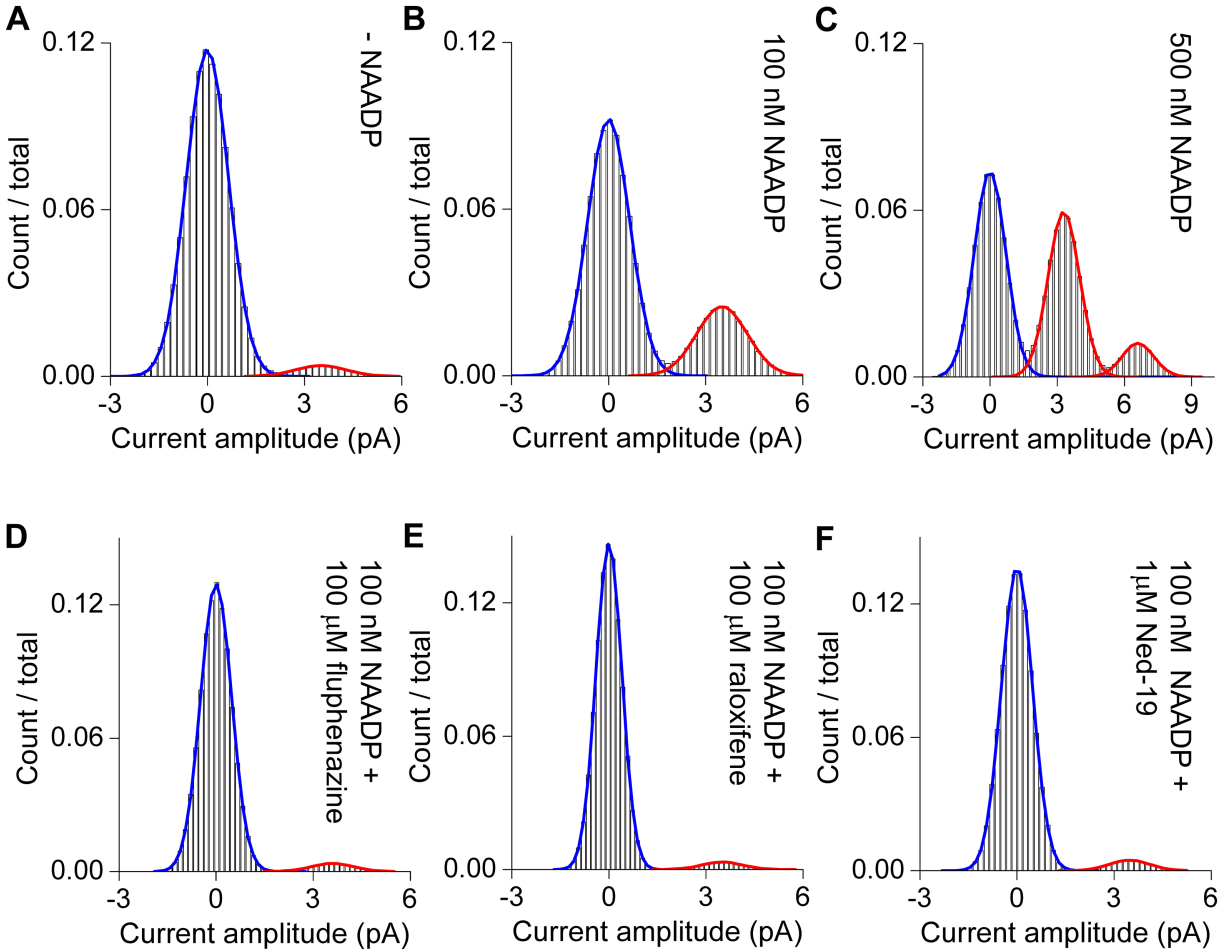
A
- NAADP
B
100 nM NAADP
C
500 nM NAADP
D
100 nM NAADP +
100 µM fluphenazine
E
100 nM NAADP +
100 µM raloxifene
F
100 nM NAADP +
1µM Ned-19
Count / total
0.12
0.06
0.00
-3
0
3
6
9
Current amplitude (pA)

Figure 8